

THE ENVIRONMENTAL DEPENDENCE OF THE EVOLVING S0 FRACTION*

DENNIS W. JUST¹, DENNIS ZARITSKY¹, DAVID J. SAND^{1,2,3}, VANDANA DESAI^{4,5}, GREGORY RUDNICK⁶

Accepted 2010 Jan 12

ABSTRACT

We reinvestigate the dramatic rise in the S0 fraction, f_{S0} , within clusters since $z \sim 0.5$. In particular, we focus on the role of the global galaxy environment on f_{S0} by compiling, either from our own observations or the literature, robust line-of-sight velocity dispersions, σ 's, for a sample of galaxy groups and clusters at $0.1 < z < 0.8$ that have uniformly determined, published morphological fractions. We find that the trend of f_{S0} with redshift is twice as strong for $\sigma < 750 \text{ km s}^{-1}$ groups/poor clusters than for higher- σ , rich clusters. From this result, we infer that over this redshift range galaxy-galaxy interactions, which are more effective in lower- σ environments, are more responsible for transforming spiral galaxies into S0's than galaxy-environment processes, which are more effective in higher- σ environments. The rapid, recent growth of the S0 population in groups and poor clusters implies that large numbers of progenitors exist in low- σ systems at modest redshifts (~ 0.5), where morphologies and internal kinematics are within the measurement range of current technology.

Subject headings: Galaxies: Clusters: General — Galaxies: Groups: General — Galaxies: evolution

1. INTRODUCTION

The fraction of galaxies morphologically classified as S0 (f_{S0}) increases by a factor of ~ 3 in galaxy groups and clusters over the past ~ 5 Gyr, at the expense of the spiral fraction (Dressler et al. 1997). This evolution has generally been interpreted as the result of the transformation of spirals into S0's within dense environments (Dressler et al. (1997); Fasano et al. (2000), hereafter F00; Smith et al. (2005); Postman et al. (2005); Poggianti et al. (2006); Desai et al. (2007), hereafter D07), although the physical mechanism remains undetermined. As highlighted by Dressler (1980), the relationship between morphologies and environment can help distinguish between hypothesized formation mechanisms for S0's. As practiced, this effort involves tracing galaxy populations as a function of environment (Dressler 1980; Postman & Geller 1984; Zabludoff & Mulchaey 1998; Helsdon & Ponman 2003), increasingly at higher redshifts (Dressler et al. 1997; Kautsch et al. 2008; Wilman et al. 2009). Those studies in turn have produced the evidence for significant evolution of the S0 fraction (Dressler et al. 1997), but have not examined whether the rate of evolution itself depends on environment.

We focus on the relationship between S0 evolution and the velocity dispersion (σ) of the group or cluster that

hosts the S0's. Processes that are expected to operate best in lower- σ environments, where the lower relative velocities between galaxies allow them to interact more effectively, include mergers and galaxy-galaxy interactions (Toomre & Toomre 1972; Icke 1985; Lavery & Henry 1988; Byrd & Valtonen 1990; Mihos 2004). Those expected to work best in higher- σ environments, either directly because of the high velocities, the deeper potential implied by the high velocities, or the higher density intracluster medium, include ram pressure stripping (Gunn & Gott 1972; Abadi et al. 1999; Quilis et al. 2000), strangulation (Larson et al. 1980; Bekki et al. 2002), and harassment (Richstone 1976; Moore et al. 1998).

To investigate the dependence of f_{S0} on environment, we return to published morphological samples. We use published visual morphological classifications as the indicator of galaxy type. Quantities related to f_{S0} , such as B/T and color distributions, have also been used to investigate such questions, but morphologies provide additional, complementary information. In fact, various recent studies are suggesting that morphological evolution is somewhat decoupled from the evolution of the stellar population (Poggianti et al. 2006; Tran et al. 2009). Morphologies are available across a significant range of redshifts and velocity dispersions, and significant effort has been expended in putting these on a common footing across redshift (F00; D07). We compile an internally-consistent set of velocity dispersions, recalculating the velocity dispersion using either previously published individual galaxy redshifts or redshifts from our own observations, to provide a measure of environment. Again, alternative measurements of environment exist, for example X-ray luminosities could have been used. However, X-ray measurements, particularly for low-mass, high-redshift environments, are scarce and velocity dispersions provide the most uniform and extensive data. Studies using different measures of either galaxy type or environment are mixed. For example X-ray luminosities correlate with B/T at $z \sim 0$ (Balogh et al. 2002) and with early-type fraction at $z > 1$ (Postman et al. 2005), but

* Observations reported here were obtained at the MMT Observatory, a joint facility of the University of Arizona and the Smithsonian Institution; and based on data collected at the Magellan Telescope, which is operated by the Carnegie Observatories.

¹ Steward Observatory, University of Arizona, 933 North Cherry Avenue, Tucson, AZ 85721, USA

² Harvard Center for Astrophysics and Las Cumbres Observatory Global Telescope Network Fellow

³ Harvard-Smithsonian Center for Astrophysics, 60 Garden Street, Cambridge, MA 02138, USA

⁴ Division of Physics, Mathematics and Astronomy, California Institute of Technology, Pasadena, CA 91125, USA

⁵ Spitzer Science Center, California Institute of Technology, Pasadena, CA 91125, USA

⁶ The University of Kansas, Department of Physics and Astronomy, Malott room 1082, 1251 Wescoe Hall Drive, Lawrence, KS 66045, USA

velocity dispersions correlate only weakly with the fraction of red galaxies within the virial radius (Balogh et al. 2004). Apparently conflicting results such as these highlight the importance of using consistent measurements of both galaxy type and environment across redshift when investigating evolution.

In §2, we describe the two samples we chose to use, the spectroscopic measurements we acquired in an attempt to obtain velocity dispersions to complete the sample, and the calculation of a consistent set of velocity dispersion measurements. In §3, we present our results, discuss their implications in §4, and summarize in §5. When computing the aperture size used for calculating the velocity dispersion, we assume $H_0 = 70 \text{ km s}^{-1} \text{ Mpc}^{-1}$, $\Omega_m = 0.3$, and $\Omega_\Lambda = 0.7$ (hereafter, the “Lambda cosmology”). However, for the aperture size within which galaxies are included in the calculation of morphological fractions, $H_0 = 50 \text{ km s}^{-1} \text{ Mpc}^{-1}$, $\Omega_m = 1$, and $\Omega_\Lambda = 0$ (hereafter, the “classic cosmology”) is assumed.

2. DATA

2.1. Sample

Morphological fractions can depend sensitively on the aperture within which cluster members are classified and on the absolute magnitude to which the classification is done. As such, it can be quite difficult, and potentially misleading, to use classifications from disparate sources. D07 presented their own classification of a set of galaxies and combined these with a set from the literature for which they were able to closely match the classification procedure, the aperture used, and the magnitude limit. Specifically, the sample presented in D07 consists of 23 galaxy clusters at $z \sim 0.1\text{--}0.5$ drawn from the F00 sample and 10 clusters at $z \sim 0.5\text{--}0.8$ drawn from EDisCS. The F00 sample in turn consists of nine clusters at $0.1 \lesssim z \lesssim 0.3$ added by the authors themselves, five clusters at $0.15 \lesssim z \lesssim 0.3$ that either appeared in Couch et al. (1998) or were classified in a manner consistent with that study, and nine clusters at $0.3 \lesssim z \lesssim 0.5$ from the MORPHS study (Dressler et al. 1997; Smail et al. 1997), all of which were classified in a consistent manner. D07 used the F00 procedure when classifying galaxies to minimize systematic differences between the two samples; in particular, the five authors who did the morphological classification also reclassified the highest redshift clusters of F00 (from $0.3 < z < 0.5$), following the same procedure as the original authors (Smail et al. 1997), and found good agreement.

Errors on the morphological fractions for those from the ESO Distant Cluster Survey (EDisCS; White et al. 2005) were computed using the method of Gehrels (1986). The situation is somewhat more complicated for the F00 morphological fractions. We calculate the uncertainties using the Gehrels method, but some of the necessary information, such as the various correction and completeness factors, are not available and we infer them indirectly from the data provided by F00. To test the sensitivity of our results to the uncertainties, we also do all the analysis described subsequently using the quoted uncertainties in F00, which were not calculated using the Gehrels method. None of the results (including the statistical significances quoted) change sufficiently between the two approaches to alter any of our conclusions. To

directly compare their results to F00, who present morphological fractions for non-uniform apertures that correspond to apertures of radii spanning from ~ 500 to 700 kpc, D07 used the classic cosmology to measure morphological fractions within fixed 600 kpc radius apertures for the EDisCS clusters. This selection of a fixed physical aperture attempts to best match, on average, the F00 measurements, which are for a range of apertures. However, D07 demonstrated that a choice of aperture that scales with R_{200} ($0.6R_{200}$) results in f_{S0} values that are in all cases within the uncertainty estimates. Lastly, regarding the magnitude limit, D07 classify galaxies down to a fixed absolute magnitude across the redshift range, chosen to match the F00 classification procedure, assuming the rest-frame colors and I -band magnitude of an elliptical galaxy (details provided in D07). Applying the incorrect cosmology (i.e. classic rather than Lambda cosmology) results in differential magnitude limits across the redshift range from 0.2 to 0.8 of a few tenths of a magnitude, comparable to the uncertainties in the observed magnitudes themselves and therefore not expected to have a noticeable effect.

A sample of $z \sim 1$ clusters with morphological classifications and redshift measurements from Postman et al. (2005) also appear in D07. However, those morphological fractions were not explicitly matched to those of F00 (i.e., by taking steps to minimize systematic differences in classification, such as those stated above) and, therefore, we exclude these clusters to avoid any possible confusion in the interpretation of our results. Including these clusters does not alter our main results.

2.2. New and Archival Redshifts

Of the 33 galaxy clusters and groups from the combined sample of F00 and EDisCS, seven ($\sim 20\%$; all from F00) do not have previously published velocity dispersion measurements. All of these clusters are at $z < 0.25$, where less than half of the clusters have velocity dispersion measurements. This important part of parameter space drives much of the $f_{S0}\text{--}z$ trend observed in F00. Although several of these clusters have enough individual galaxy redshifts available in the literature with which to calculate a reliable velocity dispersion ($\gtrsim 10$, see Beers et al. 1990), we still targeted them for observation because a higher number of redshifts allows us to calculate a more robust velocity dispersion. We targeted six clusters (Abell 951, Abell 1643, Abell 1878, Abell 1952, Abell 2192, and Abell 2658) using Hectospec (Fabricant et al. 2005) on the MMT between 2007 November to 2008 April. We observed each cluster for a total of 30–60 minutes and measured redshifts using the IRAF task *rvsao*. We used HSRED (e.g., §3.2 of Papovich et al. 2006) for the Hectospec data reduction. We also targeted four clusters (Abell 1878, Abell 3330, Cl0054–27, and Cl0413–6559) using the Inamori-Magellan Areal Camera and Spectrograph (IMACS; Bigelow et al. 1998) on the Magellan Baade telescope during two observation runs in 2008 June and 2008 September. IMACS data was reduced using the COSMOS package⁸, following standard reduc-

⁸ The Carnegie Observatories System for Multiobject Spectroscopy was created by A. Oemler, K. Clardy, D. Kelson, and G. Walth. See <http://www.ociv.edu/Code/cosmos>.

TABLE 1
LOG OF OBSERVATIONS

Cluster	Date	Telescope	Instrument	Total Redshifts Measured	Cluster Redshifts Measured	Notes
Abell 951	2007 Nov	MMT	Hectospec	23	19	...
Abell 2658	2007 Oct	MMT	Hectospec	146	41	...
Abell 1952	2008 Mar	MMT	Hectospec	131	46	...
Abell 2192	2008 Mar	MMT	Hectospec	100	13	...
Abell 1643	2008 Mar	MMT	Hectospec	Lost due to weather.
Abell 1878	2008 Apr	MMT	Hectospec	Lost due to weather.
	2008 Jun	Magellan	IMACS	25	18	...
Cl0054–27	2008 Jun	Magellan	IMACS	Lost due to weather.
Abell 3330	2008 Sep	Magellan	IMACS	Lost due to weather.
Cl0413–6559	2008 Sep	Magellan	IMACS	Lost due to weather.

tion procedures. Based on our comparison of 15 objects for which previous redshift measurements exist, we calculate that our velocity measurement uncertainty is 86 km sec^{-1} . This is a conservative estimate in that we assign the entire difference between our measurements and the published ones to ourselves.

A log of the observations of the clusters is presented in Table 1. The target galaxies are selected from the NASA Extragalactic Database (NED) and so there is no uniform selection criteria. We prioritize what appear to be early-type galaxies and use whatever other information is in NED to maximize our return on cluster members, but given the heterogeneity of the source material the target sample is ill-defined. Furthermore, as with all multiobject spectroscopy, the effective selection is complicated by fiber/slit allocation algorithms and then by the intrinsic spectrum of an object. In detail, such biases can lead to differences in measured velocity dispersions due to differences in the dispersions of different morphological types within a cluster (cf. Zabludoff & Franx 1993), but here we use the velocity dispersions only as a rough ranking of environment and are not interested in differences at the $\sim 10\%$ level. Both of these spectrographs provide large (> 24 arcmin) wide fields-of-view, so the galaxies sample the dynamics well beyond the cluster core. These observations provide enough redshifts for all but one cluster (Abell 1643 from the F00 sample, which was observed during poor weather) to measure the velocity dispersions for nearly the full sample (32/33 clusters). The other clusters lost due to weather had enough redshifts to reliably measure the velocity dispersion. In the analyses that follow, only these 32 clusters are included.

In all, we present new redshift measurements for five clusters (four from Hectospec observations and one from IMACS observations). Although this is a small number of clusters relative to the entire sample, they lie in the region of parameter space responsible for much of the S0 evolution (i.e., low- z , high- f_{S0}). In addition to these new redshift measurements, we took advantage of the large number of previously-measured redshifts available in the literature. These redshifts came from various studies, and we used NED to search for and select the data. This provides improved velocity dispersion measurements for many of the clusters.

2.3. Velocity Dispersion Measurements

We calculate velocity dispersions for the entire sample, including those with previously measured velocity disper-

sions, so that all measurements for the velocity dispersion are calculated using the same method. We now describe our procedure for evaluating the velocity dispersion, including our iterative procedure to define an aperture. In the end, we find that the velocity dispersions have only a slight dependence on the aperture as long as the aperture is a significant fraction of the virial radius.

Starting with both the literature and newly-measured redshifts, we include only those galaxies within 3 Mpc of the cluster center in our initial estimate of the velocity dispersion, although we do not always have spectroscopic redshifts out to that radius. The cluster center is as defined in the previous studies and remains unchanged through our procedure. Because of the small number of spectroscopic members in most of these clusters and the nature of the iterative procedure, we use the initial center, which is often defined either by X-ray contours, brightest cluster galaxy, or weak lensing contours rather than from the galaxy population centroid. Following Halliday et al. (2004), we also apply a redshift cut of $\Delta z = 0.015$ about the redshift of the cluster. Only redshifts from the literature with quoted errors $\lesssim 0.01$ are included; a difference in redshift of 0.01 corresponds to 3000 km s^{-1} , which is much larger than the velocity dispersion itself for even our richest clusters. We use the biweight statistic of Beers et al. (1990) to calculate the value of σ , which gives robust velocity dispersion measurements with as few as ~ 10 galaxy redshift measurements. The velocity dispersions are corrected to be rest-frame velocity dispersions. Regarding our choice of initial aperture, we find that varying it within the range $\sim 1.5\text{--}3$ Mpc affects the velocity dispersion by $\lesssim 10\%$ for all our clusters, most often $\lesssim 5\%$. In fact, the velocity dispersion calculated within any aperture varying from $\sim 1.5\text{--}3$ Mpc (when not implementing our iterative aperture scheme outlined below) changes by $\lesssim 15\%$ for all our clusters except Abell 951 and Abell 2658, whose velocity dispersions change by $\sim 50\%$ within that range. After calculating the velocity dispersion, 3σ outliers are rejected and the process iterated until no outliers remain (see §5.2 of Halliday et al. 2004). This value of σ is then used to calculate an estimated virial radius, R_{200} , using Equation (5) of Finn, Zaritsky, & McCarthy (2004):

$$R_{200} = 1.73 \frac{\sigma}{1000 \text{ km s}^{-1}} [\Omega_{\Lambda} + \Omega_0(1+z)^3]^{-1/2} h_{100}^{-1} \text{ Mpc.} \quad (1)$$

A new cut is applied at R_{200} , and the process iterated until convergence. Sometimes R_{200} is greater than 3 Mpc,

TABLE 2
MAIN PROPERTIES OF THE SAMPLE

Name (1)	z (2)	σ (3)	R_{200} (4)	N_{iter} (5)	N_{mem} (6)	f_E (7)	f_{S0} (8)	f_S (9)	f_{E+S0} (10)	Sample (11)
A3330	0.091	732^{+237}_{-82}	1.73	...	9	$0.307^{+0.089}_{-0.070}$	$0.501^{+0.083}_{-0.084}$	$0.193^{+0.085}_{-0.055}$	$0.807^{+0.056}_{-0.085}$	1
A389	0.116	662^{+175}_{-130}	1.55	3	40	$0.353^{+0.099}_{-0.088}$	$0.629^{+0.087}_{-0.087}$	$0.019^{+0.070}_{-0.074}$	$0.981^{+0.014}_{-0.070}$	1
A951*	0.143	537^{+128}_{-66}	1.24	4	23	$0.313^{+0.127}_{-0.095}$	$0.649^{+0.098}_{-0.129}$	$0.038^{+0.096}_{-0.031}$	$0.962^{+0.031}_{-0.096}$	1
A2218	0.171	1520^{+112}_{-74}	3.45	1	98	$0.437^{+0.092}_{-0.085}$	$0.240^{+0.090}_{-0.067}$	$0.324^{+0.083}_{-0.085}$	$0.677^{+0.085}_{-0.083}$	1
A1689	0.181	1876^{+98}_{-71}	4.24	1	206	$0.363^{+0.063}_{-0.051}$	$0.363^{+0.063}_{-0.051}$	$0.274^{+0.059}_{-0.048}$	$0.726^{+0.048}_{-0.059}$	1
A2658*	0.185	498^{+99}_{-58}	1.12	...	15	$0.491^{+0.121}_{-0.152}$	$0.410^{+0.152}_{-0.119}$	$0.099^{+0.130}_{-0.062}$	$0.901^{+0.062}_{-0.130}$	1
A2192*	0.187	635^{+139}_{-112}	1.43	...	16	$0.287^{+0.085}_{-0.076}$	$0.511^{+0.077}_{-0.099}$	$0.202^{+0.095}_{-0.054}$	$0.798^{+0.054}_{-0.095}$	1
A1643	0.198	$0.242^{+0.070}_{-0.073}$	$0.476^{+0.075}_{-0.090}$	$0.282^{+0.075}_{-0.075}$	$0.718^{+0.075}_{-0.075}$	1
A1878*	0.222 ^a	828^{+280}_{-135}	1.83	1	13	$0.364^{+0.106}_{-0.083}$	$0.282^{+0.070}_{-0.104}$	$0.354^{+0.116}_{-0.073}$	$0.646^{+0.073}_{-0.116}$	1
A2111* ^b	0.229	1129^{+121}_{-80}	2.49	2	80	$0.465^{+0.066}_{-0.067}$	$0.336^{+0.064}_{-0.063}$	$0.200^{+0.064}_{-0.047}$	$0.800^{+0.047}_{-0.064}$	1
A1952*	0.248	718^{+293}_{-209}	1.57	1	18	$0.413^{+0.078}_{-0.078}$	$0.380^{+0.072}_{-0.081}$	$0.207^{+0.082}_{-0.052}$	$0.793^{+0.052}_{-0.082}$	1
AC118	0.308	1748^{+99}_{-139}	3.69	1	83	$0.246^{+0.061}_{-0.053}$	$0.527^{+0.062}_{-0.064}$	$0.227^{+0.062}_{-0.049}$	$0.773^{+0.049}_{-0.062}$	1
AC103	0.311	965^{+132}_{-81}	2.03	1	55	$0.301^{+0.078}_{-0.071}$	$0.313^{+0.086}_{-0.064}$	$0.386^{+0.075}_{-0.081}$	$0.614^{+0.081}_{-0.075}$	1
AC114	0.315	1889^{+81}_{-74}	3.98	1	196	$0.223^{+0.049}_{-0.051}$	$0.318^{+0.061}_{-0.050}$	$0.459^{+0.060}_{-0.058}$	$0.541^{+0.058}_{-0.060}$	1
Cl1446+2619	0.370	1397^{+287}_{-218}	2.85	2	20	$0.338^{+0.082}_{-0.070}$	$0.248^{+0.074}_{-0.068}$	$0.415^{+0.086}_{-0.072}$	$0.585^{+0.072}_{-0.086}$	1
Cl0024+1652	0.391	764^{+40}_{-50}	1.54	2	235	$0.348^{+0.084}_{-0.076}$	$0.227^{+0.075}_{-0.070}$	$0.426^{+0.082}_{-0.085}$	$0.574^{+0.085}_{-0.082}$	1
Cl0939+4713	0.405	1331^{+96}_{-109}	2.65	1	72	$0.250^{+0.095}_{-0.068}$	$0.257^{+0.100}_{-0.070}$	$0.493^{+0.086}_{-0.086}$	$0.507^{+0.086}_{-0.100}$	1
Cl0303+1706	0.418	769^{+120}_{-94}	1.52	2	56	$0.227^{+0.084}_{-0.072}$	$0.126^{+0.075}_{-0.054}$	$0.647^{+0.085}_{-0.088}$	$0.353^{+0.088}_{-0.085}$	1
3C295	0.461	1907^{+142}_{-205}	3.69	1	32	$0.463^{+0.093}_{-0.101}$	$0.197^{+0.095}_{-0.067}$	$0.341^{+0.100}_{-0.086}$	$0.659^{+0.086}_{-0.100}$	1
Cl0412-6559	0.510	626^{+210}_{-179}	1.17	1	19	$0.347^{+0.089}_{-0.089}$	$0.090^{+0.064}_{-0.053}$	$0.564^{+0.080}_{-0.105}$	$0.437^{+0.105}_{-0.080}$	1
Cl1601+42	0.539	749^{+97}_{-76}	1.38	1	55	$0.509^{+0.064}_{-0.068}$	$0.165^{+0.061}_{-0.042}$	$0.326^{+0.068}_{-0.058}$	$0.674^{+0.058}_{-0.068}$	1
Cl0016+16	0.545	1307^{+112}_{-113}	2.41	2	99	$0.502^{+0.076}_{-0.080}$	$0.208^{+0.076}_{-0.055}$	$0.291^{+0.074}_{-0.069}$	$0.709^{+0.069}_{-0.074}$	1
Cl0054-27	0.560	700^{+284}_{-254}	1.28	2	17	$0.310^{+0.087}_{-0.077}$	$0.246^{+0.084}_{-0.073}$	$0.444^{+0.085}_{-0.092}$	$0.556^{+0.092}_{-0.085}$	1
Cl1138-1133	0.480	746^{+96}_{-79}	1.43	1	49	$0.305^{+0.164}_{-0.120}$	$0.095^{+0.113}_{-0.084}$	$0.600^{+0.145}_{-0.162}$	$0.400^{+0.162}_{-0.145}$	2
Cl1232-1250	0.541	1171^{+155}_{-70}	2.16	1	54	$0.350^{+0.040}_{-0.040}$	$0.170^{+0.030}_{-0.030}$	$0.470^{+0.040}_{-0.040}$	$0.530^{+0.040}_{-0.040}$	2
Cl1037-1243	0.578	344^{+73}_{-64}	0.58	1	16	$0.281^{+0.124}_{-0.146}$	$0.000^{+0.109}_{-0.000}$	$0.625^{+0.138}_{-0.156}$	$0.281^{+0.124}_{-0.146}$	2
Cl1227-1138	0.636	584^{+93}_{-70}	0.64	...	22	$0.290^{+0.165}_{-0.136}$	$0.146^{+0.157}_{-0.095}$	$0.394^{+0.167}_{-0.164}$	$0.436^{+0.160}_{-0.162}$	2
Cl1054-1146	0.697	603^{+170}_{-140}	1.01	2	33	$0.245^{+0.071}_{-0.069}$	$0.000^{+0.036}_{-0.000}$	$0.755^{+0.069}_{-0.071}$	$0.245^{+0.071}_{-0.069}$	2
Cl1103-1245b	0.703	235^{+203}_{-86}	0.39	...	9	$0.250^{+0.120}_{-0.080}$	$0.000^{+0.070}_{-0.000}$	$0.750^{+0.080}_{-0.120}$	$0.250^{+0.120}_{-0.080}$	2
Cl1040-1155	0.704	535^{+89}_{-71}	0.89	2	15	$0.377^{+0.136}_{-0.116}$	$0.066^{+0.093}_{-0.058}$	$0.419^{+0.141}_{-0.115}$	$0.444^{+0.141}_{-0.123}$	2
Cl1054-1245	0.750	570^{+141}_{-103}	0.93	2	22	$0.300^{+0.107}_{-0.090}$	$0.270^{+0.104}_{-0.087}$	$0.433^{+0.108}_{-0.102}$	$0.567^{+0.102}_{-0.108}$	2
Cl1354-1230	0.762	732^{+233}_{-48}	1.18	1	21	$0.170^{+0.070}_{-0.050}$	$0.290^{+0.070}_{-0.060}$	$0.550^{+0.080}_{-0.070}$	$0.450^{+0.070}_{-0.080}$	2
Cl1216-1201	0.794	1066^{+82}_{-84}	1.69	1	67	$0.490^{+0.030}_{-0.020}$	$0.220^{+0.020}_{-0.020}$	$0.270^{+0.020}_{-0.020}$	$0.710^{+0.020}_{-0.020}$	2

NOTE. — (1) Cluster Name. An asterisk (*) denotes a cluster with new data; (2) Redshift; (3) Velocity Dispersion in units of km s^{-1} ; (4) Virial Radius in units of Mpc; (5) Number of iterations until convergence, see §2.3; (6) Number of redshifts ultimately used in calculating the value in Column 3; (7) Fraction of Elliptical galaxies; (8) Fraction of S0 galaxies; (9) Fraction of Spiral galaxies; (10) Fraction of Elliptical+S0 galaxies; (11) Sample, 1-Fasano et al. (2000), 2-EDisCS

^a This redshift is different than that which appears in F00, who use $z = 0.254$. The origin of the discrepancy can be traced back to Sandage, Kristian, & Westphal (1976), where two potential redshifts for the cluster are given at $z = 0.222$ and $z = 0.254$. The lower value was assumed to be foreground, so the latter value was adopted in later studies. However, with our newly measured redshifts of 18 galaxies near the cluster position that are within ± 0.015 of the lower value and only 2 that are within ± 0.015 of the higher value, we adopt $z = 0.222$ as the cluster redshift.

^b While no new redshifts have been measured for this cluster, it's velocity dispersion has not been published as far as the authors know, and is presented for the first time here.

resulting in more redshifts being included in the later iterations. The main properties of our 32 cluster sample, including these new velocity dispersion measurements, appears in Table 2. The values for R_{200} , the number of iterations until convergence, N_{iter} , and the number of redshifts used in the final iteration, N_{mem} , appear in Columns 4, 5, and 6, of Table 2, respectively. For five of the clusters, Abell 3330, Abell 2658, Abell 2192, Cl1103-1245b, and Cl1227-1138, this process of iteration removes galaxy redshifts until there are too few ($\lesssim 10$) to reliably calculate a velocity dispersion. For these systems, the velocity dispersion is calculated using a fixed 3 Mpc cut, and the R_{200} that appears in Table 2 is calculated from Equation (1) using the velocity disper-

sion obtained with that aperture. We estimate the 1σ errors by selecting random subsamples of the data from which to evaluate the velocity dispersion.

For three of the clusters, Abell 1952, Cl0024+1652 (both part of the F00 subsample), and Cl1037-1243 (part of the EDisCS subsample), there is clear⁹ evidence of substructure in their phase-space plots. We remove

⁹ For Cl1037-1243, the substructure only becomes obvious after the first iteration. Two galaxies located $2''$ apart on the sky have velocities of ≈ -1500 and -2000 km s^{-1} relative to the cluster. Due to the relatively few galaxies in the cluster (16), these two galaxies change the velocity dispersion from ≈ 300 to 650 km s^{-1} when they are included (such that they are then not excluded in the 3σ clipping). Inspection of the histogram leads us to believe the former value is more accurate, although adopting the latter

by hand the galaxies belonging to these subgroups when calculating the velocity dispersion for the three clusters. Aside from this step, the velocity dispersion is calculated using the same procedure outlined above.

We present velocity histograms for the clusters in Figure 1 (placed at the end of the paper). The bin size is set to one-third the velocity dispersion, and the redshifts plotted are those that remain after the various cuts/iterations in the calculation (see above). Overplotted on each panel is a Gaussian with the measured velocity dispersion, normalized to the area of the histogram. Our newly calculated velocity dispersions are in good agreement with those previously measured for the EDisCS clusters (Halliday et al. 2004; Milvang-Jensen et al. 2008), but tend to give larger values for some of the $\sigma > 1000 \text{ km s}^{-1}$ F00 clusters (see D07, and references therein). This discrepancy is not due to aperture-size effects, but more likely from the different methods employed in calculating the velocity dispersion. Although the velocity dispersion was calculated using the Lambda cosmology, while the morphological fractions were calculated within an aperture defined by the classic cosmology, we find that the value of σ is fairly insensitive to aperture size (see above).

Lastly, we address the impact of observational uncertainties on our measured velocity dispersions. As mentioned previously, comparison of our redshift measurements with those in the literature suggests a single measurement uncertainty of 86 km s^{-1} . This is likely to be a significant overestimate for most systems, but we use this value to estimate the impact on the dispersions. If we simply add random velocities using a Gaussian with this σ to an intrinsic Gaussian of width commensurate to the line-of-sight velocity distribution of a specific group and cluster, we find that even in for our lowest velocity dispersion system (C11102-1245b) the observational errors inflate the dispersion by less than 20 km s^{-1} . This uncertainty is in all cases significantly less than the quoted errors on the velocity dispersion and does not affect our results.

3. RESULTS

We explore the environmental dependence (characterized by velocity dispersion) of the apparent evolution of f_{S0} with redshift (Figure 2). Our sample spans a range of dispersions from that typical of groups ($\sim 200\text{--}500 \text{ km s}^{-1}$) to poor clusters ($\sim 500\text{--}750 \text{ km s}^{-1}$) to rich clusters ($\gtrsim 750 \text{ km s}^{-1}$). Although there is no strict rule for what velocity dispersion constitutes a group versus a cluster, in what follows we use the above convention.

3.1. Analysis of the Full Sample

We begin by determining whether a relationship between f_{S0} and environment (velocity dispersion) exists across the full redshift range. Due to the selection criteria for the F00 sample (clusters were selected based on being “well-studied”), it is possible that some unappreciated selection bias manifests itself as a correlation between f_{S0} and z . Figure 6 of D07 shows a weak trend between f_{S0} and σ , although they were limited to the subset of F00 clusters with dispersion measurements and

value does not significantly change our results.

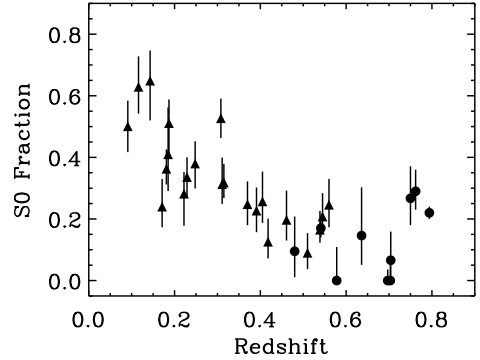


FIG. 2.— S0 Fraction (f_{S0}) plotted against redshift. Triangles represent F00 systems, while circles represent EDisCS systems.

as we have noted earlier some of the most interesting clusters were missing such measurements.

In Figure 3, we present f_{S0} plotted against velocity dispersion for our sample. Although the $f_{S0}\text{--}z$ trend in Figure 2 appears much stronger than any trend between f_{S0} and σ in Figure 3, we quantify which is the more dominant with a partial correlation analysis. The partial correlation coefficient ρ ,

$$\rho = \frac{r_{A,B} - r_{A,C}r_{B,C}}{\sqrt{(1 - r_{A,C}^2)(1 - r_{B,C}^2)}}, \quad (2)$$

is useful for disentangling the interdependence between three variables (A, B, and C), where one wants to account for the influence of the third variable (C) on the correlation of the first two. It is normalized to +1 for a perfect correlation, 0 for no correlation, and -1 for a perfect anticorrelation between A and B after accounting for C. However, the distribution of ρ does not approximate a normal distribution, so we follow the work of Kendall & Stuart (1977) in using a statistic $Z_{B,C}$, where B is the dependent variable and C is the controlled variable. $Z_{B,C}$ is defined as

$$Z_{B,C} = \frac{1}{2} \ln \left(\frac{1 + \rho}{1 - \rho} \right). \quad (3)$$

with a variance $\sigma_Z^2 = 1/(N - 2)$, where N is the number of data points. The more positive (negative) the value of $Z_{B,C}$ the stronger the correlation (anticorrelation). We treat z and σ as the independent and controlled variable, and then vice-versa. We find a stronger correlation for f_{S0} with redshift than with σ , with $Z_{z,\sigma} = -0.91 \pm 0.18$ and $Z_{\sigma,z} = -0.02 \pm 0.18$.

3.2. Analysis of Groups vs. Clusters

The results of the previous correlation analysis do not necessarily imply that environment (velocity dispersion) plays no role. From Figure 3, it is apparent that there is a wide spread in f_{S0} below $\sim 750 \text{ km s}^{-1}$ and a much narrower spread above. We therefore split the sample into a high- σ bin and a low- σ bin at this value to investigate the effect of environment on the $f_{S0}\text{--}z$ relation. This choice divides the sample into nearly equal parts as well as into samples that are more typical of groups/poor clusters ($\sigma \lesssim 750 \text{ km s}^{-1}$) and rich clusters ($\sigma \gtrsim 750 \text{ km s}^{-1}$).

Some of the clusters have suspiciously high velocity dispersions ($\sigma \gtrsim 1500 \text{ km s}^{-1}$) and are presumably unrelaxed systems (e.g., A1689). Nevertheless, given our gross binning scheme they are still likely to be systems with $\sigma \gtrsim 750 \text{ km s}^{-1}$ and placed in the appropriate velocity dispersion bin. Selecting a boundary anywhere up to 1050 km s^{-1} or down to 650 km s^{-1} (after which the number of clusters in the low- σ bin drops sharply) leaves the results that follow qualitatively unchanged, as does removing the clusters with $\sigma \gtrsim 1500 \text{ km s}^{-1}$ from the analysis.

In Figure 4, we show f_{S0} plotted against redshift in the high- σ and low- σ bins. While the f_{S0} - z trend is evident in the groups/poor clusters, the correlation appears to be much weaker, if present at all, in the rich clusters. Using uncertainty-weighted least-squares fitting, we find that the slope for the groups/poor clusters, -0.75 ± 0.14 , is steeper than the slope for the rich clusters, -0.18 ± 0.09 (a 3.4σ difference in slope). For the high- σ clusters, one may worry that there is only one data point at $z > 0.6$, which has an anomalously small error of ± 0.02 and therefore strongly influences the slope. To explore the impact of this one cluster on the fit, we have assigned it an uncertainty equal to the scatter in f_{S0} for the high- σ clusters, ± 0.07 . With this larger uncertainty estimate the new slope is -0.38 ± 0.13 , resulting in only a 1.9σ difference in slope between the low- and high- σ clusters. To bolster the case for the flat relationship among the massive clusters, we compare the morphological fractions to those from Postman et al. (2005). Although we argued in §2.1 against using these clusters for our statistical analyses, they support our finding that the relationship with redshift is nearly flat for massive clusters (Figure 4). We conclude that the difference in behavior between the low and high- σ clusters is not the result of the one high- z EDisCS cluster. Lastly, the two lowest- σ clusters in the EDisCS sample have $f_{S0} = 0$ and are potentially very unusual, although excluding them from this analysis does not alter the results.

The clusters driving most of the trend in the groups/poor clusters are the high- f_{S0} systems at low z . Among those at $z < 0.3$, there is an apparent dichotomy between those with a dense concentration of ellipticals toward the cluster center and those less centrally concentrated, in the sense that the latter have higher f_{S0} (F00). Therefore, it is also possible that S0 evolution depends further on an environmental property marked by the distribution of cluster ellipticals. Even so, there is an increase in f_{S0} since $z \sim 0.5$ (F00) when considering the high- and low-elliptical concentration systems separately.

In Figure 5, we show the elliptical fraction (f_E) plotted against redshift for the entire sample, the low- σ subsample, and the high- σ subsample. In all three cases, there is no significant trend of f_E with redshift. This argues against a misclassification between S0's and ellipticals as the origin of the S0 evolution.

4. DISCUSSION

As we have described, previous studies have found a factor of ~ 3 increase in f_{S0} between $z \sim 0.5$ and $z \sim 0$, with a corresponding decrease in the spiral fraction and a constant elliptical fraction (Dressler et al. 1997; Fasano et al. 2000). Some authors (e.g., Andreon 1998) have noted that the trends, which at some level

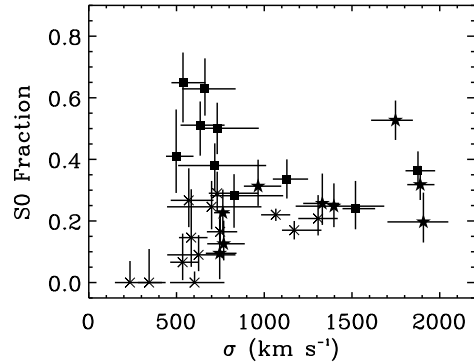


FIG. 3.— S0 fraction (f_{S0}) plotted against galaxy cluster velocity dispersion (σ). There is no simple correlation between these quantities but clearly a divergence of f_{S0} at low σ . The clusters with $z < 0.3$ (squares) are entirely non-MORPHS clusters from F00, the clusters from $0.3 < z < 0.5$ (stars) are mostly MORPHS clusters from F00, and the clusters with $z > 0.5$ (crosses) are mostly EDisCS clusters from D07.

must be affected by selection effects and methodology, may be a result of unappreciated biases. The ability to distinguish between S0's and ellipticals at higher redshifts, or other problems associated with morphological classification, could in principle result in spurious correlations. With this specific issue in mind, we investigate the relationships of various morphological fractions with redshift and velocity dispersion. We have already argued against a redshift-dependent classification problem in E's vs S0's (see above). What if there is an analogous problem with environment? For example, if ellipticals are more common in the more massive environments to the limits of our classification, and if a constant fraction of those are misclassified as S0's, then f_{S0} would appear higher in more massive environments. For Figure 5 we also conclude that there is no discernible difference in the f_E as a function of environment over the range of environments explored here.

We now remove the ellipticals from consideration and consider a plot similar to Figure 4 in which we replace the ordinate, f_{S0} , with $N_{S0}/(N_S + N_{S0})$, where N_{S0} and N_S are the numbers of S0's and spirals in each cluster, respectively (Figure 6). The dichotomy in the rate of evolution between low- σ groups/poor clusters and high- σ rich clusters remains, with slopes of -1.19 ± 0.24 and -0.07 ± 0.17 , respectively (a 3.8σ difference in slope). The difference between the morphological fractions of the two environments at low redshifts indicates that the morphological distinction between spirals and S0's is reflecting a true underlying difference between the two environments. The difference in evolutionary trends does not, unfortunately, necessarily imply that the trends are unaffected by misclassification; if the two environments have different intrinsic fractions of spirals and S0's, then redshift-dependent misclassification could affect each environment differently.

Given the results described so far, we interpret (as others before have, e.g. Dressler et al. 1997; Fasano et al. 2000; Smith et al. 2005; Poggianti et al. 2006) that the evolving S0 fraction represents the transformation of spirals into S0's. The difference here is that the S0 evolution (over these redshifts) is taking place primarily in

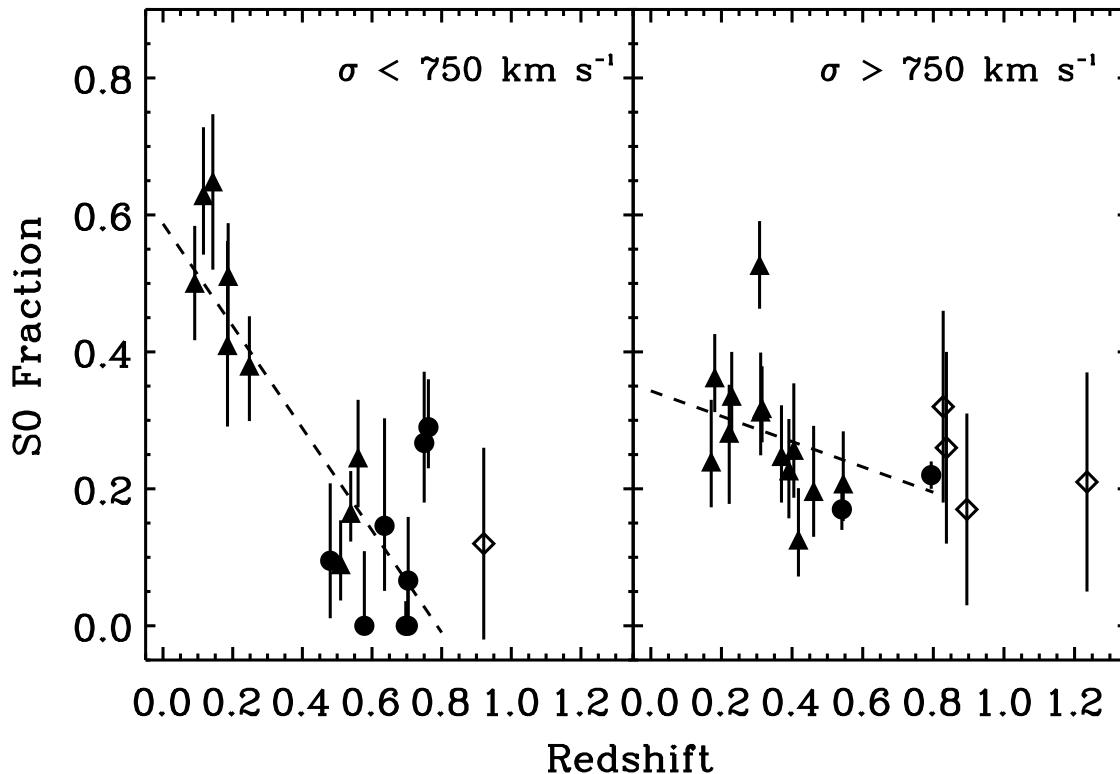


FIG. 4.— S0 Fraction plotted against redshift in a low-mass, $\sigma < 750 \text{ km s}^{-1}$ bin (*left*) and a high-mass, $\sigma > 750 \text{ km s}^{-1}$ bin (*right*) for the F00 and EDisCS clusters (triangles and circles, respectively); this binning roughly splits the sample into groups/poor clusters and rich clusters, respectively. The trend is clear in the groups/poor clusters sample (with a slope of -0.75 ± 0.14), but hardly evident in the rich clusters (with a slope of -0.18 ± 0.09), consistent with the idea that morphological transformation is taking place in group/poor cluster environments over this redshift range. The subset of clusters from Postman et al. (2005) with velocity dispersion measurements are plotted as open diamonds; these clusters are *not* used in the fits for reasons given in §2.1 and are shown for illustrative purposes only.

groups/poor clusters with $\sigma \lesssim 750 \text{ km s}^{-1}$ (Figure 4), suggesting that this is the location of S0 formation. This result then supports the hypothesis that direct galaxy interactions, i.e. mergers and/or close tidal encounters, are the dominant mechanisms in converting spirals into S0's over the redshift interval examined. The value of σ where galaxy-galaxy processes dominate and where galaxy-environment process dominate is not theoretically well constrained. Although we choose a cutoff at 750 km s^{-1} to divide the sample into equal parts, and expect mergers and/or tidal interactions to dominate in the low- σ subsample, the division into two subsamples only crudely reflects a distinction of environments where different physical effects may dominate. However, the existence of high f_{S0} systems with low velocity dispersions demonstrates that *neither* the nature or nurture of massive environments is necessary to the formation of S0's.

The conclusion that groups are the site of S0 formation, and therefore that mergers/interactions are the formation mechanism, has been arrived at in various ways. Wilman et al. (2009) find a high f_{S0} already in place in $z \sim 0.5$ groups. Poggianti et al. (2009) find more-pronounced S0 evolution in clusters with $\sigma \lesssim 800 \text{ km s}^{-1}$ by comparing a $z \sim 0$ sample to a high- z sample, although their inclusion of the same EDisCS clusters means the results are not entirely independent from ours. More

distinctly, Christlein & Zabludoff (2004) find that S0's differ from normal spirals due to a higher bulge luminosity rather than fainter disks, and interpret this as requiring bulge growth during S0 formation. They conclude that such formation mechanisms as strangulation and ram pressure stripping are therefore disfavored. Hinz et al. (2003) argue that the large scatter they measure in the local S0 Tully-Fisher relation support formation mechanisms that kinematically disturb the galaxies, i.e. interactions. The unique aspect of our observations is that we establish both the redshift and the environment at which this formation is occurring. Thereby, we identify the exact place to focus further investigation and perhaps distinguish the progenitors. Fortunately, this evolution happens at redshifts that are relatively easily accessed with current technology.

Although S0 evolution is seen primarily in the low- σ clusters and the values of f_{S0} reach between 0.5 and 0.6 at $z \sim 0$, the rate of S0 formation must reverse itself at some low value of the velocity dispersion so as not to overpopulate the field with S0's (the local field $f_{S0} \sim 0.10$; Sandage & Tammann 1987). Determining this transitional value of the velocity dispersion would further aid our understanding of the environmental processes at work. For example, one might find that this velocity dispersion corresponds to that of environments where the probability of interactions in a Hubble time

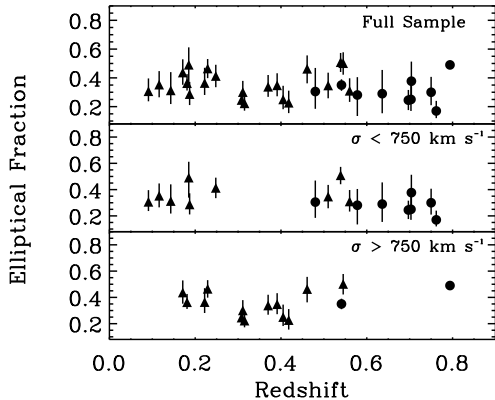


FIG. 5.— Elliptical fraction (f_E) plotted against redshift for the full sample (*top*), the low-mass, $\sigma < 750 \text{ km s}^{-1}$ bin (*middle*), and the high-mass, $\sigma > 750 \text{ km s}^{-1}$ bin (*bottom*). Symbols are the same as in Figure 2. Neither the full sample nor the subsamples show a significant trend in elliptical fraction with redshift.

become unlikely (e.g. slightly more massive than the Local Group). Our lowest- z clusters extend down to $\sim 500 \text{ km s}^{-1}$, while the $z \sim 0$ clusters of Poggianti et al. (2009) probe down to $\sim 400 \text{ km s}^{-1}$, setting an upper limit on where the trend must reverse (our two lowest velocity dispersion systems, both with $\sigma < 400 \text{ km s}^{-1}$, but high redshifts, have $f_{S0} \sim 0$, perhaps suggesting where this turnover occurs).

So far, we have not accounted for the effects of the hierarchical growth of groups and clusters on the question of S0 evolution. Groups and clusters grow over time, accreting galaxies from the field and/or groups, so that systems at $z \sim 0.8$ with a particular value of σ do not correspond to those of the same σ at $z = 0$. It has generally been assumed, due to the expectation that S0's would be rarer in low density environments, that any accretion these systems experience would be S0-poor, hence the need to transform some fraction of these galaxies into S0's. From Figure 4, we now know that this is not the case, at least for $z < 0.3$. In fact, at low z it appears that high- z clusters could increase their f_{S0} over time by accreting these smaller systems without requiring any morphological transformation mechanism. How much of the observed f_{S0} - z trend in the high- σ rich clusters could simply be due to the accretion of smaller, S0-rich groups/poor clusters similar to those in our low- σ subsample?

To estimate the increase in the number of cluster galaxies with redshift, we note that the mass of rich clusters at $z \sim 0.5$ typically increases $\sim 40\%$ by $z = 0$ (Wechsler et al. 2002), and assume that this increase in mass corresponds to the same relative increase in the number of cluster galaxies. We also assume that the mass accretion comes in the form of our low- σ groups. To the degree that field galaxies, with their lower f_{S0} , account for the accreted mass then this model will be an overestimate of the effect. The final S0 fraction $f_{S0,z=0}$ in this simple model is

$$f_{S0,z=0} = \frac{f_{S0,z=0.5} + \eta f_{S0,gr}}{1 + \eta}, \quad (4)$$

where $f_{S0,z=0.5}$ is the S0 fraction of the cluster at $z = 0.5$, η is the fractional increase in number of cluster galaxies from $z = 0.5$ to $z = 0$, i.e. $\eta = 0.4$ based on the

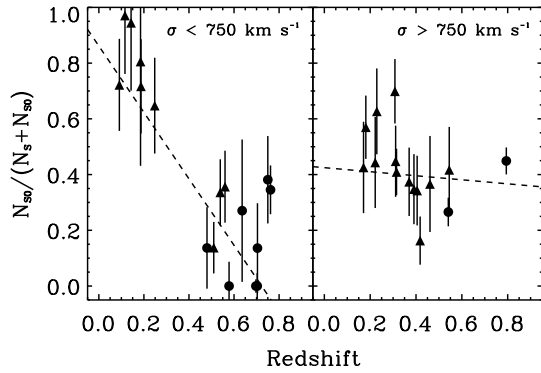


FIG. 6.— $N_{S0}/(N_S + N_{S0})$, where N_{S0} and N_S are the numbers of S0's and spirals, respectively, plotted against redshift in the low-mass, $\sigma < 750 \text{ km s}^{-1}$ bin (*left*) and the high-mass, $\sigma > 750 \text{ km s}^{-1}$ bin (*right*). The dashed line shows best-fit trends, with significantly different slopes of -1.19 ± 0.24 and -0.07 ± 0.17 (a 3.8σ difference in slope) in the left and right panels, respectively. Symbols are the same as in Figure 2.

Wechsler et al. (2002) models, and $f_{S0,gr}$ is the S0 fraction for low- z groups, for which we adopt a conservative value of 0.4. From our best-fit trend in the high- σ panel of Figure 4, the S0 fraction for a massive cluster at $z = 0.5$, $f_{S0,z=0.5}$, is 0.25. Using Equation (4) gives $f_{S0,z=0} \approx 0.3$, consistent with our best-fit trend at $z = 0$. Therefore, this simple model suggests that the trend of increasing f_{S0} with z in the high- σ clusters *could* be accounted for solely by the accretion of S0-rich groups. Regardless of the actual accretion history, we conclude that the accretion of at least some S0-rich groups will explain part of the increase in f_{S0} in clusters.

The results presented here (and elsewhere) that S0 galaxies are forming at relatively low redshifts ($z < 0.5$) and in low- σ groups, implies that we should be able to identify and study both the progenitor class and the galaxies undergoing this transition. Post-starburst galaxies are commonly suspected to be late-time examples of the latter (Dressler et al. 1985; Couch & Sharples 1987; Yang et al. 2004, 2006). If so, this transformation affects both the morphology and stellar population of the galaxy and we expect based on our results that 1) S0's in rich clusters at $z = 0$ will have mostly old stellar populations ($\gtrsim 7 \text{ Gyr}$) because most of their S0 population has been in place since $z \sim 0.8$ and 2) the S0's in low- σ , $z = 0$ clusters will have a mix of young and old stars, with roughly 50% of the S0's having a significant fraction of their stars that are younger than $\sim 3 \text{ Gyr}$ old (evidence for some relatively young S0 galaxies in the field now exists; Moran et al. 2007; Kannappan et al. 2009).

5. CONCLUSION

By compiling a large set of clusters with both internally-consistent morphological classifications and uniform velocity dispersions, σ , we examined the rate of change in the S0 fraction, f_{S0} , with redshift as a function of environment. We show that for our entire sample f_{S0} is primarily correlated with redshift and not significantly correlated with velocity dispersion. However, the evolution of f_{S0} with redshift is much stronger among $\sigma < 750 \text{ km s}^{-1}$ galaxy groups/poor clusters than in higher- σ rich clusters. We interpret this result to mean

that direct processes like galaxy mergers, which are expected to dominate in lower- σ environments, are the primary mechanisms for morphological transformation over the redshift range explored, $0 < z \lesssim 0.8$.

Further studies would benefit from a larger sample size, in particular having f_{S0} and σ measurements for both groups/poor clusters and rich clusters with comparable numbers across a similar range in redshift. This study highlights the importance of having velocity dispersion measurements in evolutionary studies, so that one can account for any environmental dependence of the evolution itself. In particular, we emphasize that more complete samples of environments are needed and that large numbers of redshifts per system are necessary to convincingly measure velocity dispersions of low-mass systems. Lastly, as emphasized by Dressler (1980) and Postman & Geller (1984), local density may be a critical factor in S0 for-

mation. We cannot measure the evolution of f_{S0} as a function of local density from our data due to the small number of spectroscopic members per system, but both larger cluster/group samples and more redshifts per system would enable such a study.

We thank the anonymous referee for insightful comments that improved the content and presentation of his paper. DJ thanks Michael Cooper for useful conversations and Daniel Christlein for helping with the Magellan observations. DZ acknowledges financial support for this work from NASA LTSA award NNG05GE82G, NASA XMM grants NNX06AG39A, NNX06AE41G, and NASA Spitzer grant 1344985. DZ also thanks the NYU Physics Department and CCPP for their hospitality during his visit.

REFERENCES

- Abadi, M. G., Moore, B., & Bower, R. G. 1999, *MNRAS*, 308, 947
 Andreon, S. 1998, *ApJ*, 501, 533
 Balogh, M. L., Baldry, I. K., Nichol, R., Miller, C., Bower, R., & Glazebrook, K. 2004, *ApJ*, 615, L101
 Balogh, M. L., et al. 2002, *ApJ*, 566, 123
 Beers, T. C., Flynn, K., & Gebhardt, K. 1990, *AJ*, 100, 32
 Bekki, K., Couch, W. J., & Shioya, Y. 2002, *ApJ*, 577, 651
 Bigelow, B. C., Dressler, A. M., Shectman, S. A., & Epps, H. W. 1998, in Presented at the Society of Photo-Optical Instrumentation Engineers (SPIE) Conference, Vol. 3355, Society of Photo-Optical Instrumentation Engineers (SPIE) Conference Series, ed. S. D'Odorico, 225–231
 Byrd, G., & Valtonen, M. 1990, *ApJ*, 350, 89
 Christlein, D., & Zabludoff, A. I. 2004, *ApJ*, 616, 192
 Couch, W. J., Barger, A. J., Smail, I., Ellis, R. S., & Sharples, R. M. 1998, *ApJ*, 497, 188
 Couch, W. J., & Sharples, R. M. 1987, *MNRAS*, 229, 423
 Desai, V., et al. 2007, *ApJ*, 660, 1151
 Dressler, A. 1980, *ApJ*, 236, 351
 Dressler, A., Gunn, J. E., & Schneider, D. P. 1985, *ApJ*, 294, 70
 Dressler, A., et al. 1997, *ApJ*, 490, 577
 Fabricant, D., et al. 2005, *PASP*, 117, 1411
 Fasano, G., Poggianti, B. M., Couch, W. J., Bettoni, D., Kjærgaard, P., & Moles, M. 2000, *ApJ*, 542, 673
 Finn, R. A., Balogh, M. L., Zaritsky, D., Miller, C. J., & Nichol, R. C. 2008, *ApJ*, 679, 279
 Finn, R. A., Zaritsky, D., & McCarthy, Jr., D. W. 2004, *ApJ*, 604, 141
 Finn, R. A., et al. 2009, in prep
 Gehrels, N. 1986, *ApJ*, 303, 336
 Gunn, J. E., & Gott, J. R. I. 1972, *ApJ*, 176, 1
 Halliday, C., et al. 2004, *A&A*, 427, 397
 Helsdon, S. F., & Ponman, T. J. 2003, *MNRAS*, 339, L29
 Hinz, J. L., Rieke, G. H., & Caldwell, N. 2003, *AJ*, 126, 2622
 Holden, B. P., et al. 2009, *ApJ*, 693, 617
 Icke, V. 1985, *A&A*, 144, 115
 Kannappan, S. J., Guie, J. M., & Baker, A. J. 2009, *AJ*, 138, 579
 Kautsch, S. J., Gonzalez, A. H., Soto, C. A., Tran, K.-V. H., Zaritsky, D., & Moustakas, J. 2008, *ApJ*, 688, L5
 Kawata, D., & Mulchaey, J. S. 2008, *ApJ*, 672, L103
 Kendall, M., & Stuart, A. 1977, *The advanced theory of statistics. Vol.1: Distribution theory*
 Larson, R. B., Tinsley, B. M., & Caldwell, C. N. 1980, *ApJ*, 237, 692
 Lavery, R. J., & Henry, J. P. 1988, *ApJ*, 330, 596
 Mihos, J. C. 2004, in *Clusters of Galaxies: Probes of Cosmological Structure and Galaxy Evolution*, ed. J. S. Mulchaey, A. Dressler, & A. Oemler, 277–+
 Milvang-Jensen, B., et al. 2008, *A&A*, 482, 419
 Moore, B., Lake, G., & Katz, N. 1998, *ApJ*, 495, 139
 Moran, S. M., Ellis, R. S., Treu, T., Smith, G. P., Rich, R. M., & Smail, I. 2007, *ApJ*, 671, 1503
 Papovich, C., et al. 2006, *AJ*, 132, 231
 Pello, R. et al. 2009, *â*, in press
 Poggianti, B. M., Smail, I., Dressler, A., Couch, W. J., Barger, A. J., Butcher, H., Ellis, R. S., & Oemler, A. J. 1999, *ApJ*, 518, 576
 Poggianti, B. M., et al. 2006, *ApJ*, 642, 188
 —. 2009, *ApJ*, 697, L137
 Postman, M., & Geller, M. J. 1984, *ApJ*, 281, 95
 Postman, M., et al. 2005, *ApJ*, 623, 721
 Quilis, V., Moore, B., & Bower, R. 2000, *Science*, 288, 1617
 Richstone, D. O. 1976, *ApJ*, 204, 642
 Sandage, A., Kristian, J., & Westphal, J. A. 1976, *ApJ*, 205, 688
 Sandage, A., & Tammann, G. A. 1987, *A revised Shapley-Ames Catalog of bright galaxies*
 Smail, I., Dressler, A., Couch, W. J., Ellis, R. S., Oemler, A. J., Butcher, H., & Sharples, R. M. 1997, *ApJS*, 110, 213
 Smith, G. P., Treu, T., Ellis, R. S., Moran, S. M., & Dressler, A. 2005, *ApJ*, 620, 78
 Toomre, A., & Toomre, J. 1972, *ApJ*, 178, 623
 Tran, K.-V. H., et al. 2009, *ApJ*, 705, 809
 Wechsler, R. H., Bullock, J. S., Primack, J. R., Kravtsov, A. V., & Dekel, A. 2002, *ApJ*, 568, 52
 White, S. D. M., et al. 2005, *A&A*, 444, 365
 Wilman, D. J., Oemler, A., Mulchaey, J. S., McGee, S. L., Balogh, M. L., & Bower, R. G. 2009, *ApJ*, 692, 298
 Yang, Y., Tremonti, C. A., Zabludoff, A. I., & Zaritsky, D. 2006, *ApJ*, 646, L33
 Yang, Y., Zabludoff, A. I., Zaritsky, D., Lauer, T. R., & Mihos, J. C. 2004, *ApJ*, 607, 258
 Yang, Y., Zabludoff, A. I., Zaritsky, D., & Mihos, J. C. 2008, *ApJ*, 688, 945
 Zabludoff, A. I. and Franx, M. 1993, *ApJ*, 106, 1314
 Zabludoff, A. I., & Mulchaey, J. S. 1998, *ApJ*, 498, L5+

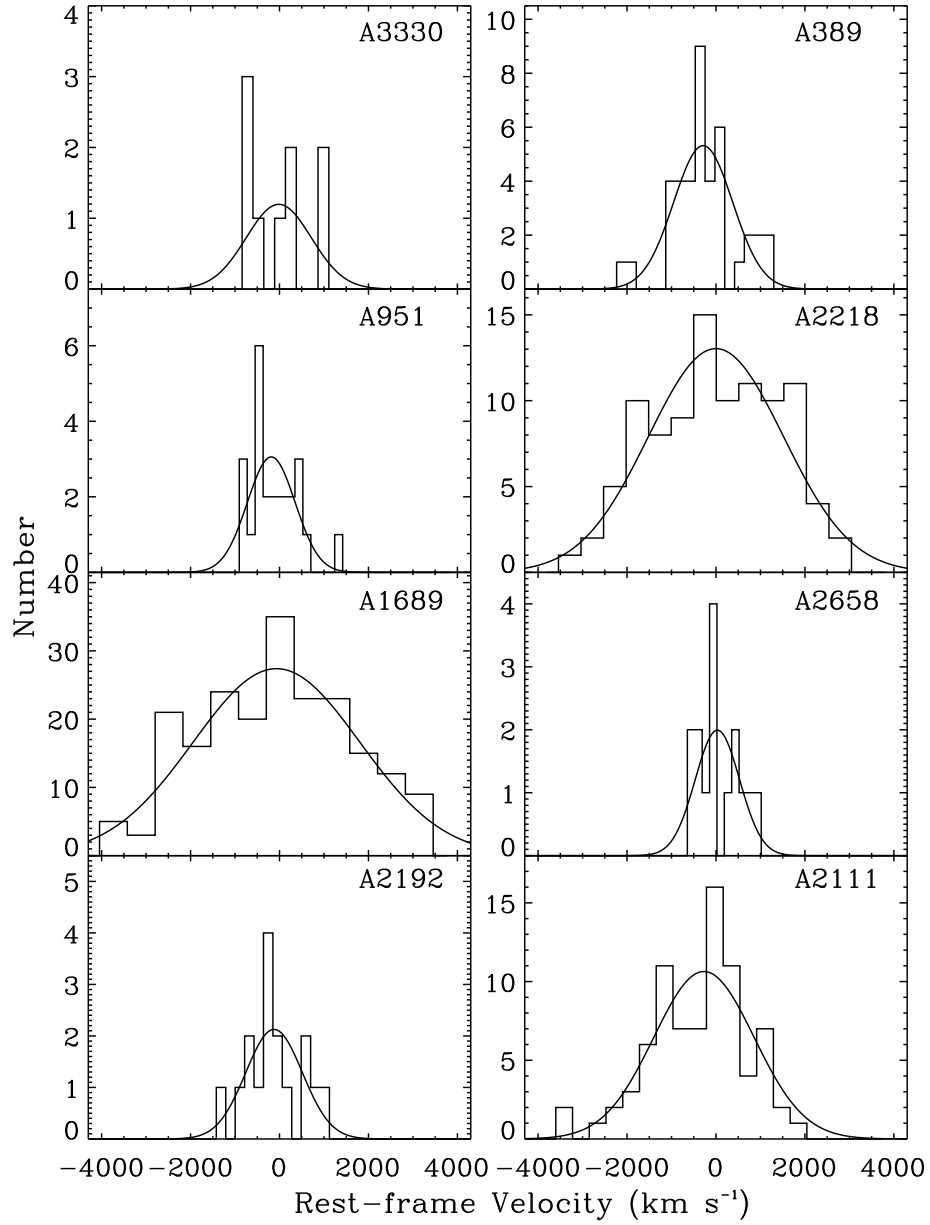
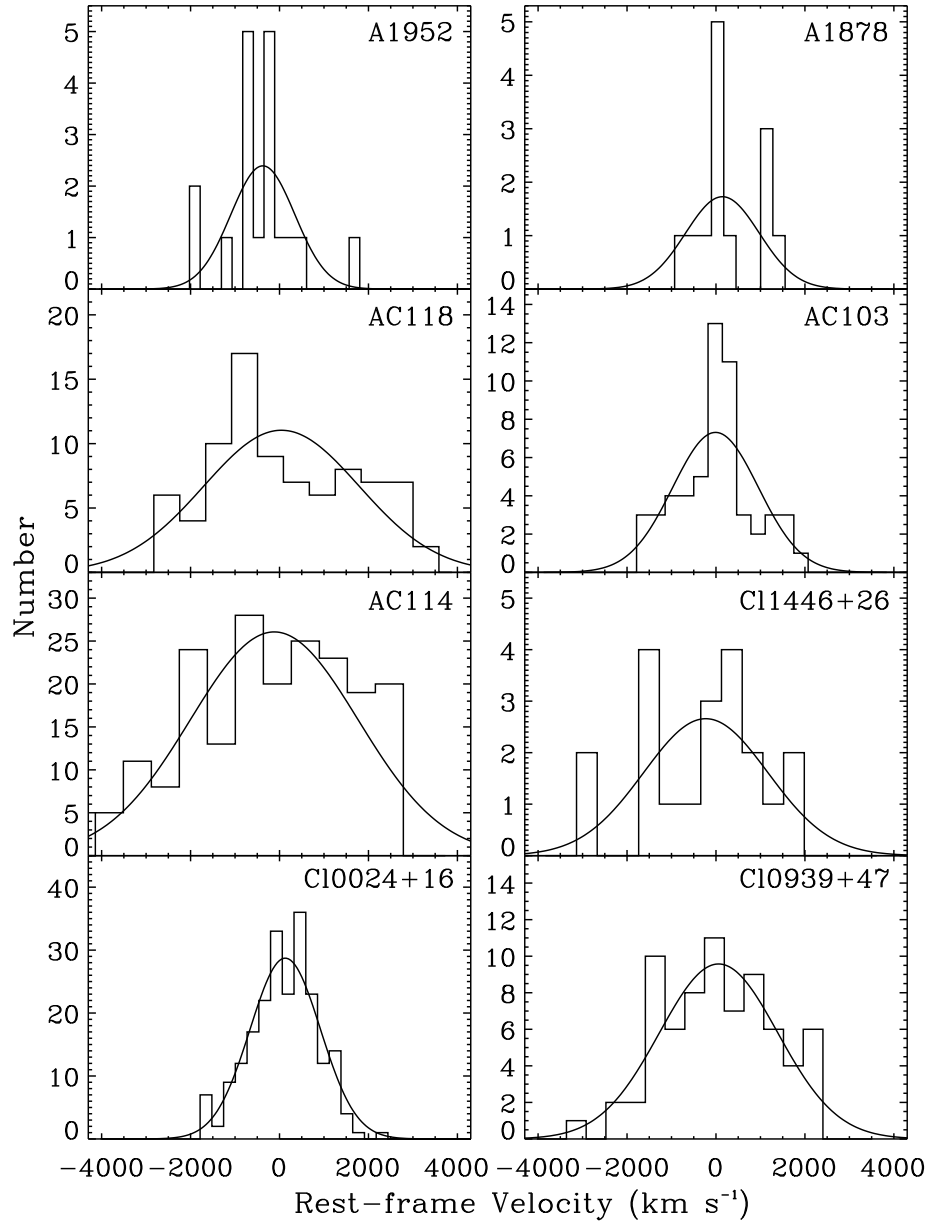
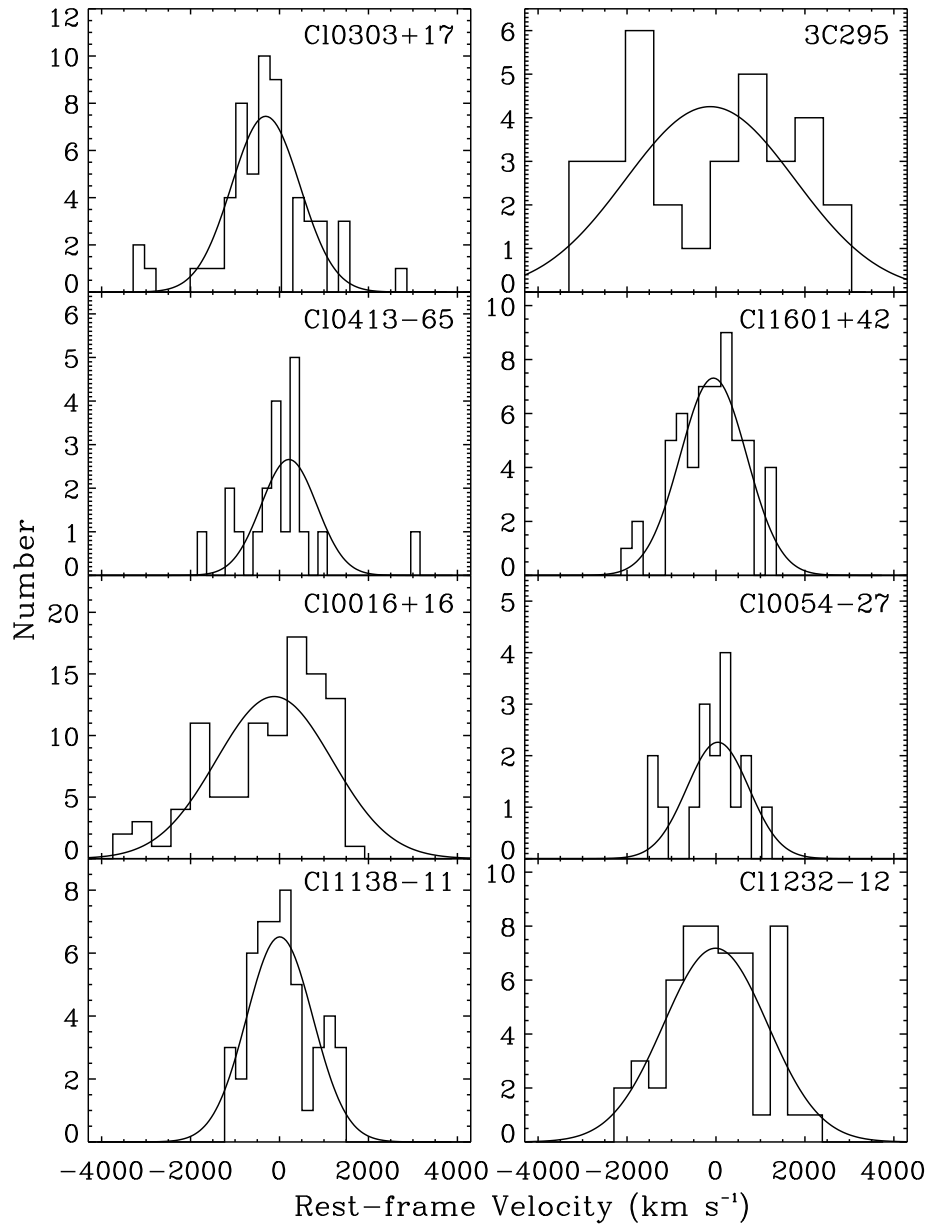
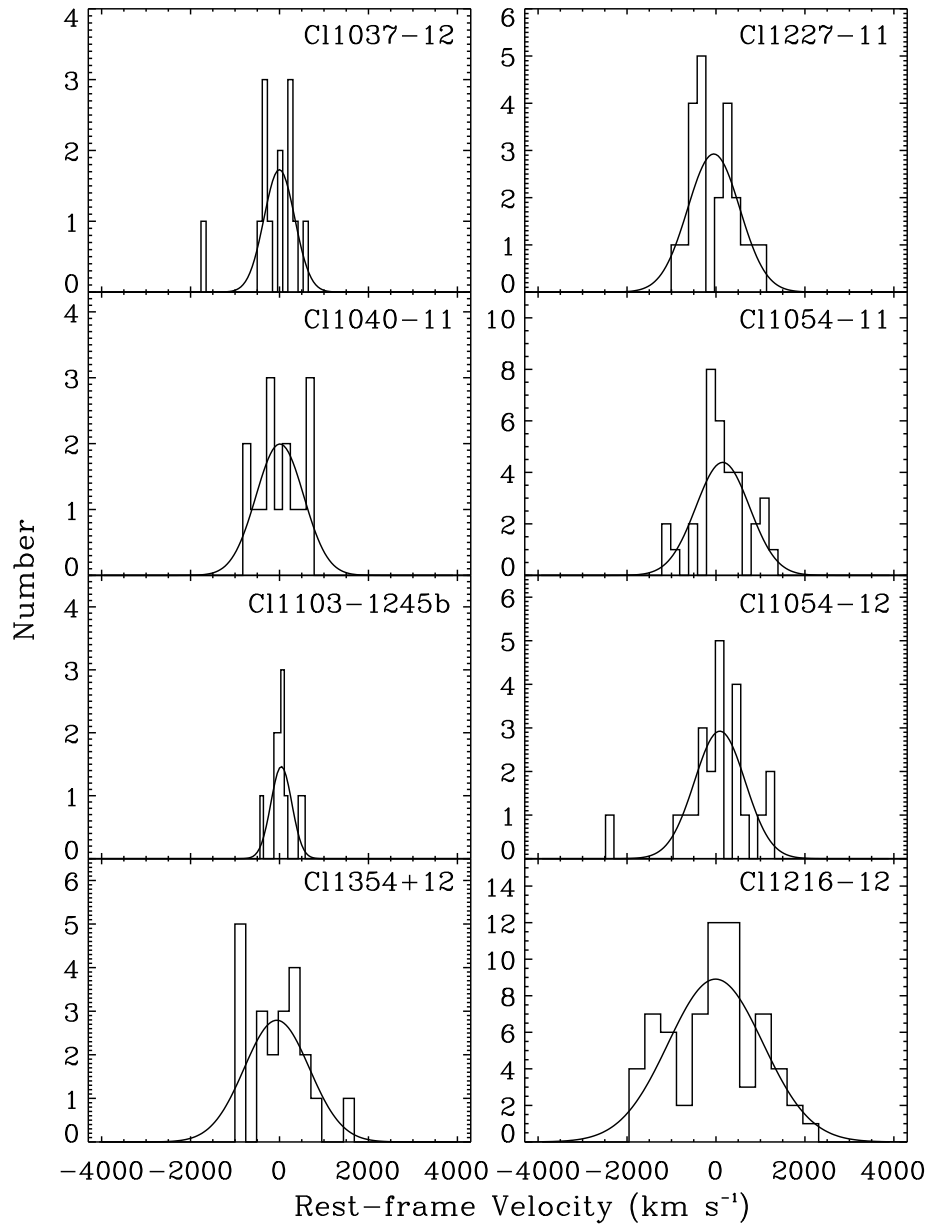


FIG. 1.— Rest-frame velocity histograms. The bin size is one-third the velocity dispersion, and the velocities plotted are those that remain after the various cuts/iterations in the calculation of σ . Overplotted on each panel is a Gaussian normalized to the area of the histogram.

FIG. 1.— *Continued*

FIG. 1.— *Continued*

FIG. 1.— *Continued*